Metal versus insulator behavior in ultrathin SrTiO_{3}-based heterostructures

Lars Bjaalie, Anderson Janotti, Burak Himmetoglu, and Chris G. Van de Walle

Phys. Rev. B **94**, 035115 — Published 7 July 2016

DOI: 10.1103/PhysRevB.94.035115

Metal versus Insulator Behavior in Ultrathin $SrTiO_3$-based Heterostructures

Lars Bjaalie, Anderson Janotti,[a] Burak Himmetoglu,[b] and Chris G. Van de Walle
Materials Department, University of California, Santa Barbara, CA 93106-5050, USA
(Dated: June 10, 2016)

Complex-oxide interfaces can give rise to two-dimensional electron gases (2DEGs) with extremely high densities: for $SrTiO_3/GdTiO_3$ (STO/GTO), a density of 1/2 electron per unit-cell area is found within the STO. In this work we use first-principles calculations to study GTO/STO/GTO heterostructures, where both interfaces contribute electrons to the STO. We find that for a thick STO layer the electrons from the interfaces delocalize over multiple TiO_2 planes. Once the STO thickness is reduced below three layers, we find that the electrons localize on every other interfacial Ti atom, leading to an insulating phase. We attribute this localization to the combination of high electron density and distortions at the interface. This is further confirmed by a model of the transition based on electron doping of bulk STO, allowing for the same type of distortions as at the interface with GTO. These findings elucidate previous observations [P. Moetakef *et al.*, *Phys. Rev. B* **2012**, *86*, 201102], but our proposed physical mechanisms are general and should apply to other complex-oxide interfaces as well.

I. INTRODUCTION

Recent experiments have revealed the formation of a two-dimensional electron gas (2DEG) at the interface between the cubic band insulator $SrTiO_3$ (STO) and the highly distorted (tilts and rotations of the TiO_6 octahedra) Mott insulator $GdTiO_3$ (GTO), with an electron density of 1/2 electron per unit-cell area.[1] The 2DEG resides on the STO side, and the electron density ($\sim 3\times10^{14}$ cm^{-2}) is more than one order of magnitude higher than those obtained using conventional semiconductors, opening a path towards novel electronic device applications. Sheet resistance measurements indicate a remarkable dependence of the electronic structure of STO/GTO heterostructures on the thickness of the STO: GTO/STO/GTO structures are metallic if the STO is three or more layers thick, but insulating for fewer layers.[2,3] Computational studies for one-layer-thick STO[4] and experimental studies for various STO thicknesses[5,6] have been reported. However, the microscopic mechanisms that trigger the dramatic change in the electronic structure with STO layer thickness are yet to be elucidated.

2DEG formation at the STO/GTO interface can be understood as follows. In STO, the valences are Sr^{2+}, Ti^{4+}, and O^{2-}; in GTO, Gd^{3+}, Ti^{3+}, and O^{2-}. Along the [001] direction, STO is non-polar since it is composed of charge-neutral $(TiO_2)^0$ and $(SrO)^0$ planes, whereas GTO is polar, composed of $(TiO_2)^-$ and $(GdO)^+$ planes. Each GdO plane donates 1/2 electron per unit-cell area to each of the adjacent TiO_2 planes. At the (001) interface, there is therefore a polar discontinuity, giving rise to an excess of 1/2 electron per unit-cell area. Since the conduction-band minimum of STO lies within the Mott Hubbard gap of GTO,[7] the excess electrons end up in the STO. Therefore, in a GTO/STO/GTO heterostructure (Figure 1), there will be an excess $2\times1/2$ electron per unit-cell area (corresponding to a 2D density of $\sim 7\times10^{14}$ cm^{-2}) in the STO.

The specific question we will address here is why and how GTO/STO/GTO structures become insulating when the STO thickness is reduced to one or two layers. We do this by using density functional theory with a hybrid functional, studying the evolution of the electronic structure as the STO thickness decreases. Hybrid functionals correctly describe the physics of these perovskite materials, including the Mott insulator GTO.[8,9] For a sufficiently high number of STO layers a 2DEG forms at each interface, but once the number of layers becomes small enough (and hence the electron density large enough) the excess electrons localize.[2,6] Our study elucidates how this insulating state is realized, and highlights the importance of coupling to lattice distortions. The insulating state is manifested in the form of electrons that become localized in the interfacial STO layers, where the material essentially transforms from an "ordinary" band insulator to a charge-ordered Mott insulator. We demonstrate how distortions of the crystal structure play a critical role in the stabilization of this Mott-insulator phase.

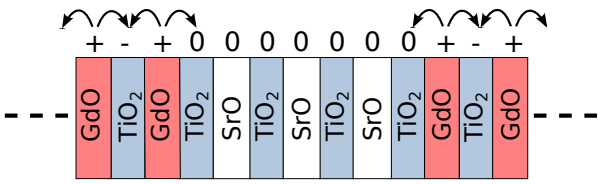

FIG. 1. Polar discontinuities in a $SrTiO_3/GdTiO_3$ double heterostructure. Arrows indicate electron transfer between planes in the polar material. At each interface, an excess 1/2 electron per unit cell area is present, giving a 2D electron density of $\sim 7\times10^{14}$ cm^{-2}.

We also demonstrate that the main features of the transition from delocalized to localized states can be explained by a model based on electron doping of bulk STO. We find that the bulk material itself displays a transition to a Mott insulator at high electron densities, when distortions are allowed. Our model actually pre-

dicts the same metallic-to-insulating behavior as a function of increasing electron density as is observed for the heterostructures as a function of STO layer thickness. This confirms that our proposed physical mechanisms are independent of the specific interface, and should apply to other complex-oxide interfaces as well.

II. METHODS AND APPROACH

Our calculations are based on density functional theory (DFT) with the Heyd-Scuseria-Ernzerhof (HSE) hybrid functional[10] and projector augmented wave (PAW) potentials[11,12] as implemented in the VASP code.[13,14] In the HSE functional, non-local Hartree-Fock exchange is mixed into the short-range exchange potential from the generalized gradient approximation (GGA),[15] and the correlation potential and the long-range part of the exchange potential are those of the GGA functional.

For the calculations of bulk materials, integrations over the Brillouin zone are replaced with sums over a mesh of 6×6×6 Γ-centered special k-points for STO, and 4×4×2 for GTO, both with a 500 eV plane-wave basis set energy cutoff. Bulk STO is stable in a cubic perovskite crystal structure at room temperature, described by a 5-atom cubic unit cell. Bulk GTO is stable in a $GdFeO_3$ crystal structure (*Pbnm* space group), described by a 20-atom orthorhombic unit cell which includes rotation and tilts of TiO_6 octahedra. The Gd $5f$ electrons are included in the core of the pseudopotential. For STO, the calculated lattice parameter of 3.903 Å is within 0.1% of the experimental value,[16] and the indirect and direct band gaps are 3.27 eV and 3.63 eV, close to the experimental values of 3.25 eV and 3.75 eV.[17]

HSE also gives an accurate description of the lattice parameters of GTO, giving 5.350 Å, 5.726 Å, and 7.624 Å, each within 0.8% of the experimental lattice parameters.[18] The band gap in GTO derives from a splitting of the Ti $3d$ derived bands into an occupied lower Hubbard (LHB) band and an empty upper Hubbard band (UHB). The LHB and UHB have relatively low dispersion, and the calculated Mott-Hubbard gap is 2.02 eV, in agreement with optical measurements.[19] These Hubbard bands occur in the same spin channel, so that the magnetic moments on the Ti atoms exhibit ferromagnetic ordering.

We investigate the evolution of the electronic structure of GTO/STO/GTO heterostructures as a function of decreasing STO thickness by carrying out calculations for $(STO)_n/(GTO)_3$ superlattices, with $n = 6$ to 1. Here a 2×2×1 k-point mesh is used with a 500 eV plane-wave cutoff for relaxations, and electronic properties are calculated with a 4×4×1 k-point mesh with a 400 eV plane-wave cutoff. The direction perpendicular to the interface is [001] in the coordinate systems of both the STO and GTO unit cells. Internal atomic positions and the lattice parameter perpendicular to the interface are allowed to relax, and each interface in the superlattice provides one excess electron going into the STO. To allow for the type of octahedral rotations and tilts as in bulk GTO, the in-plane area is thus $\sqrt{2}a \times \sqrt{2}a$, where we fix a to the lattice parameter of STO. Experimental layer structures may be strained, for instance due to growth on LSAT substrates.[2] It is known that strain can affect the electronic structure of complex oxide heterostructures.[20] We have verified that the conclusions presented in this paper remain unchanged when the layers are strained to LSAT.

Symmetric interfaces allow for faster convergence of the charge density than non-symmetric, and we therefore use an odd number of GTO layers. In the [001] direction, the distortions of the octahedra create an $ABA...$ stacking, with the letters corresponding to the tilt/rotation pattern of each GTO layer. For an odd number of layers there will be a plane of symmetry in the middle of the GTO, whereas for an even number of layers this symmetry is broken. We use three GTO layers, and a comparison between $(STO)_1/(GTO)_3$ and $(STO)_1/(GTO)_5$ superlattices indicates that a greater GTO thickness leads to very small changes in the electronic and atomic structure: the width of the GTO LHB changes by less than 0.02 eV, and bond angles by less than 0.5°.

The Gd $5f$ electrons have a substantial magnetic moment, and interact with the electronic states in the STO through antiferromagnetic Gd-O-Ti interactions across the interfaces. The difference in the total energy between different magnetic configurations of the electrons in the STO is on the order of 10 meV per Ti atom, which is many times smaller than the energy difference between metallic and insulating phases. Therefore, neglecting the influence of the Gd $5f$ electrons on the electronic states in the STO by including them in the core of the pseudopotential is a good approximation.

III. RESULTS

A. Thick STO layers: Metal

We start by presenting the results for thicker STO layers. In Figure 2(a) we show the electronic band structure of $(STO)_6/(GTO)_3$ in the energy range comprising the LHB and UHB of GTO, also encompassing the STO conduction band. Our results show that $(STO)_6/(GTO)_3$ has a metallic state confined to the STO layer, indicative of the 2DEG. The STO subbands can be clearly distinguished from the GTO LHB, which consists of four bands derived from the $3d$ states associated with the four Ti atoms within the bulk GTO. We note that there is a sizable spin splitting of the STO conduction band, with the great majority of the electrons in the 2DEG occupying spin-up bands, and a small fraction occupying spin-down bands near the Fermi level. The spin splitting is in fact so large that the partially occupied STO conduction band overlaps the GTO LHB.

The crystal structure and the electronic charge density associated with the STO subbands in the

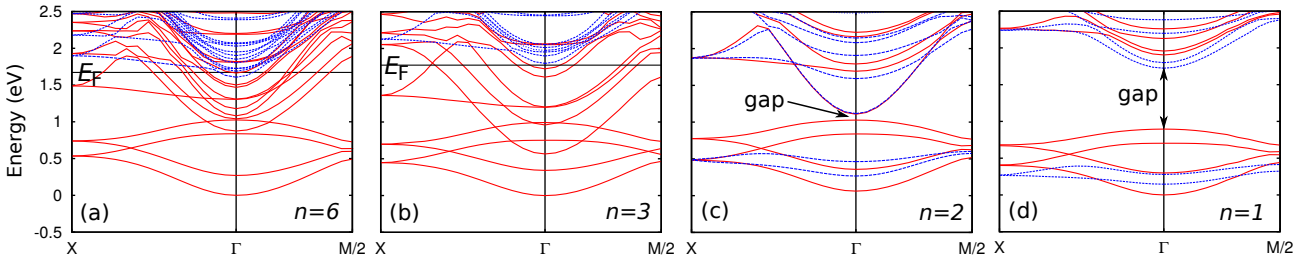

FIG. 2. Electronic band structure of $(GdTiO_3)_3/(SrTiO_3)_n$ superlattices for (a) n=6, (b) n=3, (c) n=2, and (d) n=1. The bands are plotted along the in-plane directions $\Gamma \rightarrow$ M/2 and $\Gamma \rightarrow$ X, where M=($\frac{1}{2}$,$\frac{1}{2}$,0) and X=($\frac{1}{2}$,0,0), with coordinates referenced to the reciprocal basis vectors of the cubic perovskite 5-atom primitive cell. The energy axis is referenced to the bottom of the $GdTiO_3$ lower Hubbard band. Solid black line indicates Fermi level in the case of metallic systems (n=6 and n=3). Red (solid) indicates spin up, and blue (dashed) indicates spin down.

$(STO)_6/(GTO)_3$ superlattice are shown in Figure 3(a). The TiO_6 octahedra in the interfacial plane on the STO side exhibit large rotations in order to accommodate the connectivity across the interface. Octahedra deeper in the STO layer are close in structure to those in bulk STO; the relaxation largely occurs within a single interface TiO_2 plane. Two electrons occupy the STO conduction band, forming a 2DEG with a density corresponding to 1/2 electrons per 5-atom unit-cell area per interface, consistent with having two identical STO/GTO interfaces.

The charge density reveals that the orbital character of the occupied subbands varies depending on the position in the structure: In the two TiO_2 planes nearest to the interface the orbital character is d_{xy}, while it is d_{yz} and d_{xz} deeper in the STO. A consequence of the different orbital character is that the planar-averaged electron density [Figure 3(b)] appears narrower and more peaked in the two TiO_2 planes nearest to the interface; the double-peaked structure in the interior of the STO reflects the d_{yz}/d_{xz} nature. Macroscopic averaging (running average along the z direction over one period of the lattice)[21] reveals, however, that the distribution of the electrons is quite uniform among the different TiO_2 planes in the STO layer.

For smaller STO thicknesses, down to $(STO)_3/(GTO)_3$, we also find a metallic ground state with integrated charge corresponding to 1/2 electron per unit-cell area per interface. For the three-layer case, the rotations of the octahedra are again large in the interfacial layer, relaxing towards cubic in the interior of the STO [Figure 4(a)]. In contrast to the six-layer case, the in-plane macroscopic average of the electron density is now distinctly higher at the interface [Figure 4(b)], with smaller contributions from the TiO_2 planes inside the STO layer.

As the thickness of the STO layer decreases, going from six to three layers, we see a downward shift of the lower-lying subbands; the overlap with the LHB is larger for the three-layer than the six-layer case. This is caused by a large spin splitting within the subbands, which increases with electron density. This large spin splitting corresponds to ferromagnetism in the STO layer, which has been observed experimentally for a $GTO/(STO)_3/GTO$ heterostructure.[22]

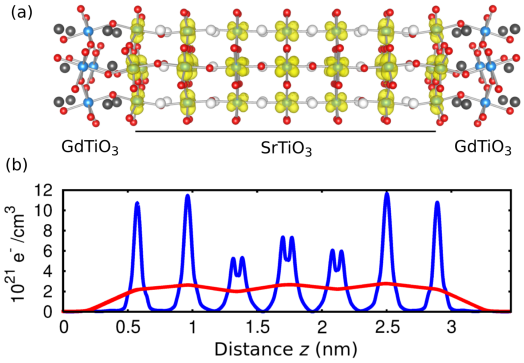

FIG. 3. (a) Charge density of the occupied $SrTiO_3$ conduction bands (isosurface plotted at 10% of maximum value) and (b) in-plane averaged electron density (blue) and macroscopic average (red) for the $(GdTiO_3)_3/(SrTiO_3)_6$ superlattice.

B. Thin STO layers: Insulator

Decreasing the STO thickness to two or one unit cells, we see a drastic change in the electronic structure: $(STO)_2/(GTO)_3$ and $(STO)_1/(GTO)_3$ are no longer metallic, and display a band gap. In the case of $(STO)_2/(GTO)_3$ we observe localization and charge-ordering of the excess electrons on every other interface Ti atom, shown in Figure 5(a). These localized states form two bands, both with spin down, which lie within the LHB of the GTO, as can be seen in Figure 2(c). Each of these two bands is associated with a single TiO_2 interface plane. The lowest- energy unoccupied band originates from the central TiO_2 plane in the STO layer, and it exhibits a large dispersion as it is composed of Ti d_{xy} states, shown in Figure 5(b). The calculated band gap is 90 meV. The octahedra within the central TiO_2 plane are practically cubic as a consequence of the STO_2/GTO_3 superlattice geometry. To check that our

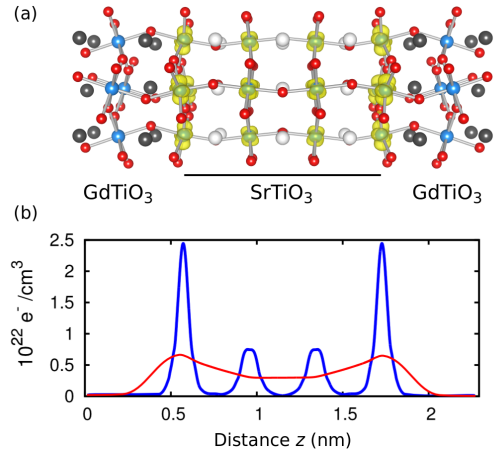

FIG. 4. (a) Charge density of the occupied $SrTiO_3$ conduction bands and (b) in-plane averaged electron density (blue) and macroscopic average (red) for the $(GdTiO_3)_3/(SrTiO_3)_3$ superlattice.

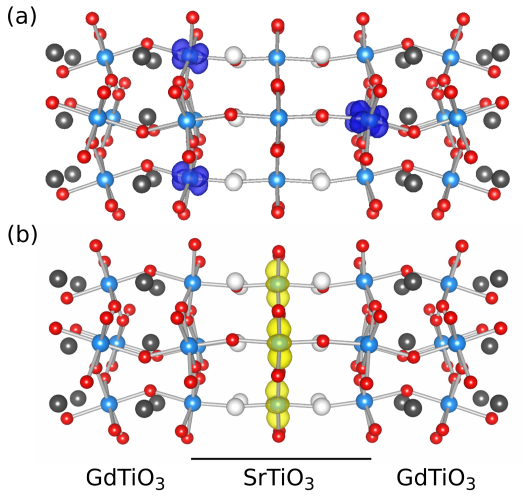

FIG. 5. Γ-point charge density of (a) the two bands occupied by the excess electrons and (b) the conduction-band minimum, for the $(GdTiO_3)_3/(SrTiO_3)_2$ superlattice. Blue indicates spin down, and yellow no spin polarization.

results were not an artifact of this imposed high symmetry, we also performed calculations for $(STO)_2/(GTO)_4$. The same localization of electrons on interfacial Ti atoms was found, with the same band gap. This result is similar to a GGA+U study on $STO/LaAlO_3$ and $STO/NdGaO_3$ superlattices (both forming polar discontinuities with excess electrons in STO),[23] indicating that the thickness-dependent metal-to-insulator transition is a general feature of STO and not dependent on the details of the interface.

In the limit of a single STO layer we also obtain an insulating ground state, in agreement with experiment.[3] In contrast to the two-layer case, we now obtain a sizeable band gap of 0.82 eV, but the nature of the insulating state is the same: the TiO_2 layers located between GdO and

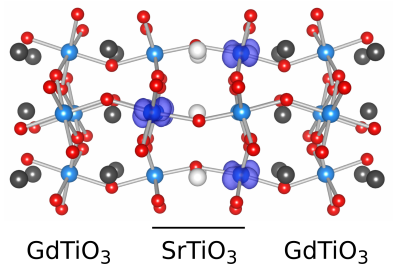

FIG. 6. Γ-point charge density of the two bands occupied by the excess electrons in $SrTiO_3$ for the $(GdTiO_3)_3/(SrTiO_3)_1$ superlattice. Blue indicates spin down.

SrO layers display large rotations of the octahedra, the excess electrons are localized on every other Ti interface atom (Figure 6), and the electrons are distributed in two bands that overlap with the GTO LHB [Figure 2(d)]. These results differ from previous theoretical work on the n=1 case, using GGA+U and a model Hamiltonian based on GGA calculations, which resulted in a dimer Mott ground state with a 0.2 eV band gap.[4]

IV. DISCUSSION

A. Understanding the transition

To understand why the system is no longer metallic for the n=2 and n=1 cases, we examine the atomic structure of the superlattices and the contributions to the total energy. First, we note that the GTO atomic structure and LHB energies remain largely intact as the thickness of the STO decreases from six to one layer—the Ti-O-Ti angles differ by less than a degree, the Ti-Ti distances by less than 0.005 Å, and the bandwidth by less than 0.1 eV. For all investigated STO thicknesses, the relaxation in Ti-O-Ti bond angles required to accommodate the connectivity of the octahedra occurs predominately right at the interface—in the octahedra between planes of SrO and GdO. These interface octahedra are thus appreciably distorted, in contrast to the cubic structure of bulk STO, and these distortions are key to understanding why the system transitions from a metal to an insulator as the thickness decreases: The distortions break the degeneracy of the t_{2g} orbitals, allowing the minimization of the strong on-site electron-electron repulsion via the localization of the 3d electrons in single orbitals, each giving rise to a single band. This localization is what we observe at the interface for the one- and two-layer cases [as can be seen in Figs. 2(c) and (d), which have two spin-down bands overlapping with the GTO LHB representing the localized interface electrons].

If the system can lower its electronic energy by localizing the excess electrons on every second interface Ti atom (alternating between Ti^{3+} and Ti^{4+}), why do we not observe this localization for *all* STO thicknesses? The

answer is that there is a structural energy penalty associated with the localization; the TiO_6 octahedra have to distort. In addition to tilts and rotations, the Ti-O bond lengths also have to change; in the interface layer the Ti^{3+} atoms have longer Ti-O bonds than the Ti^{4+} atoms. For $n = 1$ ($n = 2$), the average Ti-O bond length is 2.05 Å (2.04 Å) for Ti^{3+} and 1.98 Å (1.98 Å) for Ti^{4+}. This bond-length disproportionation reflects a lowering of the symmetry compared to bulk GTO, in which each TiO_6 octahedron has the same three sets of Ti-O bond lengths. In the metallic cases, the disproportionation is not observed. Here, the bond lengths are the same for both unique interface Ti atoms. The difference in the bond length observed for $n = 1$ and $n = 2$ thus arises from the electron localization, not from the interface geometry. These changes in bond lengths cost energy, and therefore localization becomes favorable only if the energy gain due to minimization of electron-electron repulsion is sufficiently large. The amount of energy gain is proportional to the magnitude of the electron density associated with a specific band. This density will be high in the case of thin STO layers, since then the number of STO conduction-band states is low and they are filled to high energies.

To quantify this argument, we inspect the $n = 2$ case. Here, in contrast to all the other STO thicknesses investigated, we can obtain both a metallic (delocalized) and insulating (localized) solution. The metallic solution has average Ti-O bond lengths in the interfacial TiO_2 layer of 2.00 Å, the same for all Ti sites, and a total energy 0.26 eV [per $(STO)_2(GTO)_3$ supercell] higher than the insulating solution. To estimate the structural energy penalty associated with localization, we remove the Ti 3*d* electrons from the system (i.e., we remove six electrons from the supercell, meaning that there are no excess electrons in STO and no LHB in GTO), and compare the energy of the metallic structure to that of the insulating structure; the former is 1.15 eV *lower* in energy. Since the *total* energy of the metallic phase is 0.26 eV higher than the insulating phase, this means that the electronic energy gained by going from a metallic to an insulating state is 0.26–(–1.15)=1.41 eV. Since the structural energy penalty is associated mainly with distortions in the interfacial layers, we expect our estimate of 1.15 eV to apply also to cases with thicker STO layers ($n > 2$); however, the amount of electronic energy gain decreases in thicker layers due to the fact that the number of STO conduction-band states increases. For $n > 2$ electrons are spread over a larger number of bands, and the electronic energy gained by localization is insufficient to overcome the energy cost of the structural rearrangement.

B. Model to describe localization versus delocalization

In the previous section we computed the energy difference between localized (insulating) and delocalized (metallic) configurations of the excess electrons in the $n = 2$ heterostructure, finding the localized configuration to be 0.26 eV lower in energy. To further elucidate the physical mechanisms involved in the balance of localization versus delocalization, we perform an analysis for *bulk* STO. We calculate the increase in total energy upon adding electrons to bulk STO, in either a localized or a delocalized configuration. By varying the added electron density q (corresponding to the excess number of electrons per Ti atom in STO in a heterostructure with layer thickness n), and comparing the energy of the localized and delocalized configurations, we can investigate when the metal-to-insulator transition occurs.

To find the energy of the delocalized configuration, $E_{\rm deloc}(n)$, for a given layer thickness n, we add $q = 1/(n+1)$ electrons (the number of excess electrons per STO Ti atom for a layer thickness n; for $n = 1$ there are *two* TiO_2 layers in the STO region) to a 5-atom unit cell of STO, and calculate the total energy ($E^q_{5,\rm tot}$). We reference this energy to the total energy of the neutral 5-atom cell ($E^0_{5,\rm tot}$) plus $q = 1/(n+1)$ electrons at the conduction-band minimum (CBM) of the neutral cell ($E_{\rm CBM}$). Since we want the calculated energy to apply to the heterostructure supercells, in which two electrons are added to the STO layer, we multiply the resulting energy difference by $2(n+1)$:

$$E_{\rm deloc}(n) = [E^q_{5,\rm tot} - (E^0_{5,\rm tot} + q \times E_{\rm CBM})] \times 2(n+1) \quad (1)$$

The result is shown as the red curve in Figure 7.

Our model does not take the effect of the variation in electrostatic potential near the interface into account. Electrons located near the interface feel an attractive potential and hence their energy is lowered by an amount that can be estimated based on the electrostatic potential obtained from our first-principles calculations. The attractive potential also increases the electron density in the region near the interface, compared to what the density would be in a uniform potential. Since the energy increases roughly quadratically with density (see Fig. 7), this non-uniform distribution leads to an increase in the energy. Both of these effects are on the order of 0.1 eV (on the scale of Fig. 7). Since they compensate each other the overall effect is modest in magnitude and we have not included it in our bulk model.

To find the energy for the localized configuration, we need to work with a unit cell of STO large enough to accommodate charge ordering and distortions. A 20-atom unit cell of STO (i.e., a $\sqrt{2} \times \sqrt{2} \times 2$ enlargement of the 5-atom unit cell) allows for such internal structural relaxations; note this is similar to crystal structure of GTO. Upon addition of two electrons to this 20-atom cell (1/2 electron per Ti atom), the material turns into a Mott insulator. The electrons localize on every other Ti atom, and the structure displays $GdFeO_3$-type distortions.[24] The energy of this structure ($E^2_{20,\rm tot}$) is again referenced to the total energy of four neutral 5-atom $E^0_{5,\rm tot}$ cells plus 2 electrons at the CBM of the neutral cell ($E_{\rm CBM}$),

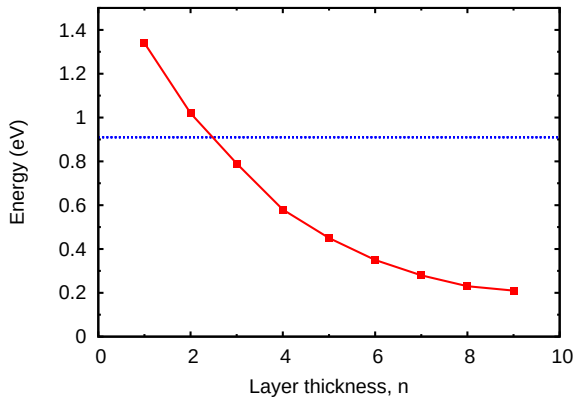

FIG. 7. Energy of a bulk model for delocalized (red) and localized (blue) configurations of a system with two excess electrons in an STO layer of thickness n. The system mimics the situation of the GTO/$(STO)_n$/GTO heterostructure with two excess electrons added per $\sqrt{2} \times \sqrt{2}$ interface area. The energies are referenced to the energy of an undistorted bulk STO crystal in which the added electrons would all be placed at the CBM. Localization is favored for systems with layer thickness $n < 3$, just like in the full heterostructures.

yielding the energy of the localized configuration:

$$E_{\rm loc} = E^2_{20,\rm tot} - [4E^0_{5,\rm tot} + 2E_{\rm CBM}] \qquad (2)$$

This energy of the localized configuration would apply to any thickness of STO in the heterostructure, since the excess electrons always localize in the interfacial TiO_2 layers, and therefore the STO layers away from the interface do not contribute.

Since the reference energy is the same for $E_{\rm deloc}$ and $E_{\rm loc}$, they can be plotted on the same energy scale, as shown in Figure 7. $E_{\rm deloc}$ decreases as the electron density decreases, corresponding to lower filling of conduction-band states. In the limit of very thick STO layers (i.e., if the added electron density q per Ti atom approaches zero), $E_{\rm deloc}$ goes to zero. For very thin layers, the localized configuration is more favorable; the crossover occurs between n=2 and n=3, which is the same thickness at which the crossover occurs in the actual heterostructures. The bulk model thus captures the key features of the behavior of thin STO layers, also indicating that the tendency for electron localization at high electron densities is independent of the nature or details of the interface.

V. CONCLUSION

We have used first-principles calculations to describe the mechanism behind the metal-to-insulator transition in GTO/STO/GTO heterostructures as the STO thickness decreases below three layers.[2] For the one- and two-layer thick STO cases, a charge-ordered ground state is found, where every other interfacial Ti atom is occupied with one $3d^1$ electron, in contrast to the delocalized ground state found for three or more STO layers. Based on a bulk model, we have shown that the localized ground state becomes favored at very high electron densities because localizing electrons in specific orbitals becomes more favorable than having to fill the conduction band up to very high energies—this in spite of the cost of the lattice distortions required to enable localization. The fact that a bulk model can reproduce the main features of the transition from metal to insulator indicates that the physical mechanisms do not depend on the specifics of the interface. This fundamental understanding of the transition is key to designing a "Mott field effect transistor" based on a GTO/STO/GTO heterostructure, where small changes in the excess electron concentration in the STO (via an applied voltage) could switch the structure between the metallic and insulating phases.

ACKNOWLEDGMENTS

We are grateful to S. Stemmer, S. J. Allen, P. Moetakef, T. A. Cain, and J. Y. Zhang for fruitful discussions. LB and AJ were supported by the NSF MRSEC Program (DMR-1121053). BH and CVdW were supported by the Center for Low Energy Systems Technology (LEAST), one of the six SRC STARnet Centers, sponsored by MARCO and DARPA. Computational resources were provided by the Center for Scientific Computing at the CNSI and MRL (an NSF MRSEC, DMR-1121053) (NSF CNS-0960316), and by the Extreme Science and Engineering Discovery Environment (XSEDE), supported by NSF (ACI-1053575 and DMR07-0072N).

[a] Current address: Materials Science and Engineering, University of Delaware, Newark, DE 19716-3106, USA
[b] Current address: Center for Scientific Computing, California NanoSystems Institute, University of California, Santa Barbara, CA 93106, USA

[1] P. Moetakef, T. A. Cain, D. G. Ouellette, J. Y. Zhang, D. O. Klenov, A. Janotti, C. G. Van de Walle, R. Siddharth, S. J. Allen, and S. Stemmer, Appl. Phys. Lett. **99**, 232116 (2011).
[2] P. Moetakef, C. A. Jackson, J. Hwang, L. Balents, S. J. Allen, and S. Stemmer, Phys. Rev. B **86**, 201102 (2012).
[3] D. G. Ouellette, P. Moetakef, T. A. Cain, J. Y. Zhang, S. Stemmer, D. Emin, and S. J. Allen, Sci. Rep. **3**, 3284

(2013).
[4] R. Chen, S. B. Lee, and L. Balents, Phys. Rev. B **87**, 161119 (2013).
[5] J. Y. Zhang, J. Hwang, S. Raghavan, and S. Stemmer, Phys. Rev. Lett. **110**, 256401 (2013).
[6] J. Y. Zhang, C. A. Jackson, R. Chen, S. Raghavan, P. Moetakef, L. Balents, and S. Stemmer, Phys. Rev. B **89**, 075140 (2014).
[7] L. Bjaalie, B. Himmetoglu, L. Weston, A. Janotti, and C. G. Van de Walle, New J. Phys. **16**, 025005 (2014).
[8] J. He and C. Franchini, Phys. Rev. B **86**, 235117 (2012).
[9] C. Franchini, J. Phys.: Condens. Matter **26**, 253202 (2014).
[10] J. Heyd, G. E. Scuseria and M. Ernzerhof, J. Chem. Phys. **118**, 8207 (2003); erratum **124**, 219906 (2006).
[11] P. E. Blöchl, Phys. Rev. B **50**, 17953 (1994).
[12] G. Kresse and D. Joubert, Phys. Rev. B **59**, 1758 (1999).
[13] G. Kresse and J. Furthmüller, Phys. Rev. B **54**, 11169 (1996).
[14] G. Kresse and J. Furthmüller, Comput. Mater. Sci. **6**, 15 (1996).
[15] J. P. Perdew, K. Burke and M. Ernzerhof, Phys. Rev. Lett. **77**, 3865 (1996)
[16] J. Brous and I. Fankuchen, E. Banks, Acta Crystallogr. **6**, 67 (1953).
[17] K. van Benthem, C. Elsässer, R. H. French, J. Appl. Phys. **90**, 6156 (2001).
[18] D. A. MacLean, H. N. Ng and J. E. Greedan, J. Solid State Chem. **30**, 35 (1979).
[19] L. Bjaalie, A. Verma, B. Himmetoglu, A. Janotti, S. Raghavan, V. Protasenko, E. H. Steenbergen, D. Jena, S. Stemmer, and C. G. Van de Walle, Phys. Rev. B **92**, 085111 (2015).
[20] N. Ganguli and P. J. Kelly, Phys. Rev. Lett. **113**, 127201 (2014).
[21] A. Baldereschi, S. Baroni and R. Resta, Phys. Rev. Lett. **61**, 734 (1988).
[22] C. A. Jackson and S. Stemmer, Phys. Rev. B **88**, 180403 (2013).
[23] D. Doennig, R. Pentcheva, Sci. Rep. **5**, 7909 (2015).
[24] L. Bjaalie, A. Janotti, B. Himmetoglu and C. G. Van de Walle, Phys. Rev. B **90**, 195117 (2014).